

SPATIALLY CORRELATED CLUSTER POPULATIONS IN THE OUTER DISK OF NGC 3184

STÉPHANE HERBERT-FORT¹, DENNIS ZARITSKY¹, JOHN MOUSTAKAS²,
DANIEL CHRISTLEIN³, ERIC WILCOTS⁴, ANDREA BARUFFOLO⁵,
ANDREA DI PAOLA⁶, ADRIANO FONTANA⁶, EMANUELE GIALLONGO⁶,
RICHARD W. POGGE⁷, ROBERTO RAGAZZONI⁵, RICCARDO SMAREGLIA⁸

¹University of Arizona/Steward Observatory, 933 N Cherry Avenue, Tucson, AZ 85721
(email: shf@as.arizona.edu)

²Center for Cosmology and Particle Physics, New York University, 4 Washington Place, New York, NY 10003

³Max-Planck-Institut für Astrophysik, Karl-Schwarzschild-Str. 1, 85748 Garching, Germany

⁴Department of Astronomy, University of Wisconsin-Madison, 475 N. Charter St., Madison, WI 53706

⁵INAF, Osservatorio Astronomico di Padova, vicolo dell'Osservatorio 5, I-35122 Padova, Italy

⁶INAF, Osservatorio Astronomico di Roma, via di Frascati 33, I-00040 Monteporzio, Italy

⁷Department of Astronomy, The Ohio State University, 140 W. 18th Avenue, Columbus, OH 43210-1173

⁸INAF, Osservatorio Astronomico di Trieste, via G. B. Tiepolo 11, I-34131 Trieste, Italy

Accepted for publication in The Astrophysical Journal

ABSTRACT

We use deep (~ 27.5 mag V -band point-source limiting magnitude) V - and U -band LBT imaging to study the outer disk (beyond the optical radius R_{25}) of the non-interacting, face-on spiral galaxy NGC 3184 ($D = 11.1$ Mpc; $R_{25} = 11.1$ kpc) and find that this outer disk contains > 1000 objects (or marginally-resolved ‘knots’) resembling star clusters with masses $\sim 10^2 - 10^4 M_{\odot}$ and ages up to ~ 1 Gyr. We find statistically significant numbers of these cluster-like knots extending to $\sim 1.4R_{25}$, with the redder knots outnumbering bluer at the largest radii. We measure clustering among knots and find significant correlation to galactocentric radii of $1.5R_{25}$ for knot separations < 1 kpc. The effective integrated surface brightness of this outer disk cluster population ranges from $30 - 32$ mag arcsec $^{-2}$ in V . We compare the H I extent to that of the correlated knots and find that the clusters extend at least to the damped Lyman- α threshold of H I column density (2×10^{20} cm $^{-2}$; $1.62R_{25}$). The blue knots are correlated with H I spiral structure to $1.5R_{25}$, while the red knots may be correlated with the outer fringes of the H I disk to $1.7R_{25}$. These results suggest that outer disks are well-populated, common, and long-lasting features of many nearby disk galaxies.

Subject headings: galaxies: individual (NGC 3184) – galaxies: star clusters – galaxies: structure – methods: statistical

1. INTRODUCTION

Ultraviolet observations with the Galaxy Evolution Explorer (GALEX; Martin et al. 2005) indicate that $\sim 30\%$ of nearby disk galaxies host star formation in an extended component (Thilker et al. 2007; Zaritsky & Christlein 2007). These stellar disks sometimes reach to more than twice the optical radius (R_{25}) and challenge our understanding of disk galaxies. Motivated by a lack of understanding and because progress here may pose additional challenges for galaxy formation models, we begin a systematic investigation of a sample of nine nearby galaxy outer disks using deep optical imaging and present first results here.

Although deep H α and broadband optical observations (e.g. Ferguson et al. 1998; Martin & Kennicutt 2001; Weiner et al. 2001) had previously detected star formation in outer disks, the ubiquity, and therefore the significance, of this component has been largely overlooked until recently. The traditional tracer of very young star clusters and ongoing star formation, H α flux, is emitted by gas surrounding a cluster for a short period of time (~ 10 Myr, or about the lifetime of massive OB stars). Consequently, the number of H α detections is modest (Ferguson et al. 1998; Martin & Kennicutt 2001; Weiner et al. 2001).

The two most prominent extended disks studied with GALEX so far, M83 and NGC 4625 (Thilker et al. 2005;

Gil de Paz et al. 2005), have nearby companions, suggesting that gravitational interactions may be responsible for their extended outer disks. A more comprehensive GALEX study (Gil de Paz et al. 2007) does contain isolated galaxies, but typically they are more distant (the majority of galaxies in the GALEX Atlas sample are > 20 Mpc away) and so only the brightest end of the knot luminosity function is sampled. To address these shortcomings, we select nearby, isolated galaxies, observe them sufficiently deeply to probe the knot luminosity function well and obtain numerous candidate knots, and develop a method to quantify the nature of the knot spatial distribution.

In complement to the imaging studies, Christlein & Zaritsky (2008) have shown that deep longslit spectroscopy can provide a measure of both the integrated extent and global disk-plane kinematics (i.e. rotation curves) of outer disks in edge-on galaxies. While spectroscopy provides useful information, it is generally limited to knots emitting H α . To expand the lookback time over which we can study disks, we image at redder colors to identify older candidate knots, but the drawback of this approach is that discrimination with background sources becomes more challenging.

Because we use optical observations to search for outer disk knots analogous to those detected by GALEX, we note the differences between the two sets of data. First,

GALEX’s spatial resolution ($\sim 5''$ FWHM) is roughly six times larger than what we typically achieve. At the distance of NGC 3184, GALEX’s resolution element corresponds to a physical scale of ~ 270 pc, compared to the ~ 40 pc of our ground-based data. GALEX knots are typically blends of multiple clusters (Gil de Paz et al. 2005), whereas (as we will show), we detect knots resembling individual star clusters. Second, GALEX observations are sensitive mainly to young clusters (< 500 Myr; Thilker et al. 2005) whereas we are sensitive to clusters with ages up to several gigayears. Finally, our mass limit is lower by a factor of 10. Our LBT data will therefore provide larger numbers of knots to use in any statistical measure of the disk.

We present the initial results of a statistical study of nearby (< 15 Mpc) outer disks, using the 8.4m Large Binocular Telescope (LBT, Mt. Graham, Arizona; Hill et al. 2006) and wide-field, prime-focus Large Binocular Cameras (LBC; Ragazzoni et al. 2006; Giallongo et al. 2008). We describe our data reduction, develop analysis tools, and apply these to deep V -band and U -band (hereafter V and U) imaging data of the nearly face-on (inclination = 17° ; Daigle et al. 2006) spiral galaxy NGC 3184 ($D = 11.1$ Mpc, or $m - M = 30.23$ mag; Leonard et al. 2002). NGC 3184 is similar to an L^* galaxy, with $M_V = -20.8$ and $M_* \sim 1.4 \times 10^{10} M_\odot$ (Moustakas et al. 2009). We demonstrate how two separate statistical methods enable us to trace outer disk cluster-like objects to large radii. Because the distance to NGC 3184 is uncertain at the $\sim 20\%$ level (~ 2 Mpc), all scales referenced to the frame of the disk are also uncertain at the $\sim 20\%$ level. This uncertainty in distance does not significantly affect our results. The detected correlation signals are independent of the physical size of the field.

We address the following questions here: 1) In a non-interacting galaxy, without an obvious population of GALEX knots, do we detect any evidence of an extended disk? 2) If so, what are the oldest clusters we detect? 3) How can we detect an older population of knots that is less distinct from the background galaxy population? 4) How does the extent of the disk compare to the fuel source (i.e. the gas).

In §2 we describe our observations, data reductions and source detections. In §3 we present color-magnitude diagrams (CMDs) of candidate outer disk sources and the range of cluster properties consistent with the candidate knots. We also present an estimate of disk knot radial extent determined from the CMDs in §3. In §4 we present a restricted three-point correlation analysis that increases contrast with the background and more effectively probes the extent of clustered outer disk objects. In §5 we present a similar clustering analysis using GALEX UV sources, and in §6 we present a comparison to the underlying neutral gas profile, using 21cm VLA data with a 3σ detection limit of $N(\text{HI}) = 6.9 \times 10^{19} \text{ cm}^{-2}$. In §7 we discuss the local environment of NGC 3184. We present a summary of our results and a brief discussion in §8.

2. OBSERVATIONS TO FINAL SOURCE CATALOG

2.1. Observations

We observed NGC 3184 with LBC-Blue on the LBT during Science Demonstration Time on March 20, 2007.

We obtained eight and nine dithered, 164-second exposures through the V and U filters, respectively, under non-photometric conditions and $\sim 0''.8$ seeing, and obtained single 164-second photometric exposures (in V and U) on February 2, 2008, together with three photometric Landolt standard star fields (Landolt 1992) for flux calibration. The photometric exposures served their purpose but due to poor image quality we exclude them from the final science mosaics.

2.2. Data Reduction

We correct for both global changes and the two-dimensional structure in the bias using a set of Interactive Data Language (IDL¹) scripts created by our group. The LBC-Blue detector array consists of four 2k x 4k CCD chips (each with a gain of ~ 1.75 electrons/ADU, read noise of ~ 12 electrons and $\sim 0''.22$ -wide pixels), three aligned side-by-side lengthwise and one centered perpendicularly above them. We begin by correcting for bias gradients along columns (spanning the long axis) in the bias frames. The median within the overscan region along each row is subtracted from that row. The overscan-corrected bias frames of each chip are then median combined after removing 1σ outliers, where σ is calculated excluding the minimum and maximum values in the stack (15 frames/stack were used). We adopt an aggressive clipping (1σ) to ensure that deviant values, which artificially increase the calculated rms value, are excluded. The result is our final ‘master bias’ frames used to subtract any residual structure in an image after the overscan levels are accounted for. We bias-correct all raw frames in this manner and trim the overscan regions.

To correct for sensitivity variations on the CCDs, we combine dithered, twilight-sky flat-field images (10 in each band). We calculate the four-chip median value of each bias-corrected flat field exposure and divide each chip of the particular four by this median level to normalize the flat. Optical distortions in LBC-Blue can result in non-flat images (a $\sim 5\%$ effect across the field of view²). We correct for this effect later using the distortion maps created by SCAMP³ (Bertin 2006) when aligning our individual images to a common field of view (see below). The normalized flats are then median combined after minimum/maximum and 1σ rejection as above, producing our ‘master flat’ for each chip. We complete our processing by dividing the bias-corrected science frames by the master flats, resulting in V images flat to $\sim 0.5\%$ and U images flat to $\sim 1\%$.

We next subtract the background level. Estimating the true background is made difficult by contaminating scattered light that varies sensitively with the telescope orientation, and by the extended galaxy that covers a large portion of the field in each exposure. To minimize the effects of these contaminants, we determine the background level in twenty 200×200 pixel regions distributed near the edges of the detector array using the IDL routine MMM⁴, which estimates the sky background in a stellar

¹ developed by Research Systems, Inc. and owned by ITT; <http://www.itervis.com/ProductServices/IDL.aspx>

² <http://lbc.oa-roma.inaf.it/commissioning/flatfield.html>

³ Version 1.4.0; <http://terapix.iap.fr/soft/scamp>

⁴ part of the Goddard IDL library, maintained by W. Landsman; <http://idlastro.gsfc.nasa.gov/>

contaminated field by assuming that contaminated sky pixel values overwhelmingly display positive departures from the true value. We then adopt the minimum background value from the regions on each chip and subtract it from that particular chip. This process is done separately for each exposure.

To create combined images free of spurious signal or cosmetic defects, we create masks of bad columns and hot pixels for each chip interactively (based on obvious defects in the flats) and invert the masks to create the weightmaps used in the combining process. Next, we reject cosmic ray detections with the IDLUTILS⁵ routine REJECT_CR (written by M. Blanton), which rejects cosmic rays by finding features sharper than the point spread function (PSF) at $> 6\sigma$ above the background. The identified cosmic ray pixels are incorporated into the bad pixel masks.

2.3. Mosaic Creation

We produce our final mosaics using SCAMP and SWarp⁶. SCAMP solves the astrometry of the dithered exposures, and requires that we first create catalogs of detected sources in each exposure. To create the necessary catalogs for SCAMP, we use SExtractor (Bertin & Arnouts 1996), restricting source detection to objects with five or more adjacent pixels for which the pixel values are at least 8σ above sky in V and 3σ above sky in U . We exclude pixels with values above 40,000 ADU when running SExtractor because these pixels produced false detections (~ 65000 ADU is the raw saturation level of the CCDs). We find that the above choices result in the best distortion maps from SCAMP (maps whose distortion level contours trace smoothly across the chip gaps), using three SCAMP iterations with tightening criteria for source matching. We use the SDSS fifth data release (DR5; Adelman-McCarthy et al. 2007) as the reference catalog to match sources in the NGC 3184 field. SCAMP provides the WCS solutions used for combining the frames with SWarp. We set the ‘EX-POTIME_KEY’ parameter in SCAMP to ‘DONTUSE’, so that the resulting fluxes are not altered by the image exposure times (we normalize the photometry to a fixed second^{-1} standard after combining the images with SWarp, when calibrating the science images to the standard star images). SCAMP is used to create the distortion maps that correct for the optical concentration effect mentioned earlier, so that the images are on the same $\sim 0''.22$ pixel^{-1} spatial scale before being combined into a mosaic.

The final step is to create the deep mosaics we use for source detection, calibration and analysis. We pass the output headers from SCAMP containing the WCS solutions of each exposure to SWarp, which we set to combine the spatially-aligned frames to their average values after accounting for the bad pixel masks. Total integration times in the deepest regions of the resulting mosaics are ~ 25 and ~ 22 minutes in V and U , respectively.

2.4. Source Detection

We build final V and U aperture photometry catalogs using SExtractor, with source detection and aper-

ture placement based on the deeper V -band mosaic (both mosaics have the same $\sim 0''.8$ PSF, and similar image quality). After trying various combinations of parameters, we select sources by identifying groups of five or more pixels each with flux $> 1\sigma$ above the background (so typical ‘detections’ are actually $> 3\sigma$, because $[\lt 0.3173]^{[\geq 5]} < 0.0032$). For our parameter choices, we set the saturation level to be 55,000 counts to conservatively avoid problematic saturated areas (we are less concerned with false detections in the mosaic, particularly with the fine-tuned settings listed below), a seeing FWHM of $0''.8$, a pixel scale of $0''.22$, local background calculation, the background manually set as 0.0 because we have already subtracted it (note that the photometry uses the local background, however), a 3×3 -pixel ‘all-ground’ convolution mask with FWHM=2 pixels for filtering to avoid spurious detections of noise peaks, a minimum contrast deblending parameter of 0.001, a ‘cleaning’ of the catalog with an efficiency parameter of 1, a background mesh size of 32 pixels, and a background-filtering mask size of 3 background meshes. Using the same SExtractor parameters, we then perform matched-aperture photometry on the U image. A visual inspection of the detected sources confirms that the above parameters lead SExtractor to detect nearly all visually-discernable objects in the region of interest, beyond the optical radius R_{25} . Our catalog becomes noticeably incomplete below $\sim 0.8R_{25}$, where SExtractor has difficulty detecting unique sources over the extended, bright emission of the inner disk.

Given the distance of NGC 3184 (11.1 Mpc, or $m - M = 30.23$ mag), our $0''.8$ seeing (~ 40 pc at the distance of NGC 3184), and that all but the brightest OB stars would fall below our detection limit (~ 27.5 mag. for the bluest sources), the candidate outer disk objects are likely to be groupings of stars. Because we detect the integrated light from members of stellar groups, or knots (see Figure 1 for examples), any photometric algorithm that requires a uniform object shape for extraction is not optimal for this work.

2.5. Photometry & Final Source Catalog

We calibrate our photometry using photometric exposures of Landolt standard star fields, taken on the same night as our individual photometric exposures of NGC 3184, to flux-calibrate the observed standard star signal for a range of airmasses and colors. We then place the photometry of eight isolated stars in the photometric frame of NGC 3184 on the standard Vega system, accounting for the calculated airmass and color terms as well as the different exposure times, and finally bootstrap the photometry of the deep mosaic using these same stars.

Colors and magnitudes are measured using circular apertures. Colors quoted throughout are from fixed four-pixel-diameter apertures ($0''.9$ or ~ 48 pc at NGC 3184, just larger than the typical $0''.8$ FWHM of detected sources), while V magnitudes are from 10-pixel-diameter apertures ($2''.24$ or ~ 121 pc at NGC 3184) and aperture-corrected using stellar curves-of-growth by -0.08 mag. Aperture corrections were calculated from eight isolated, unsaturated stars measured in 15 apertures spanning 2 – 50 pixels in diameter (or $0''.4 - 11''.2$).

⁵ http://spectro.princeton.edu/idlutils_doc.html

⁶ Version 2.17.1; <http://terapix.iap.fr/soft/swarp>

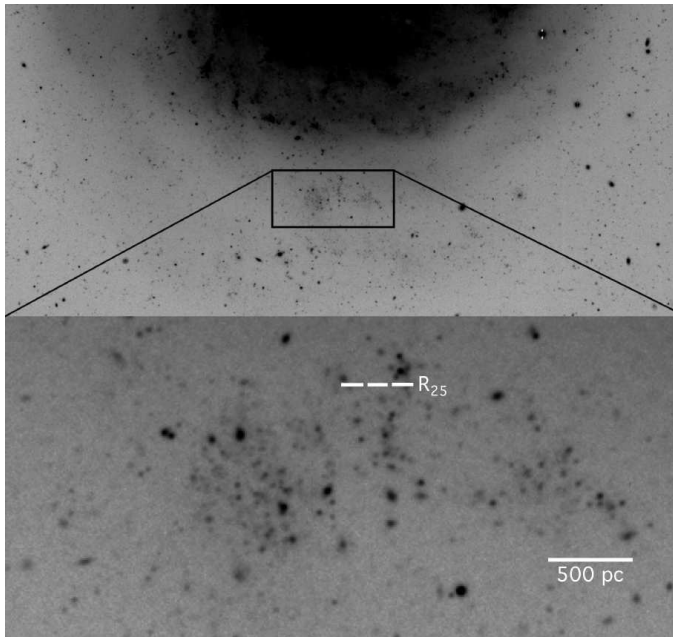


FIG. 1.— A portion of our deep V -band mosaic, with a zoom-in on a complex of faint knots near the optical radius. The optical radius (R_{25}) and a 500 pc scale bar are shown in white in the lower image. Many of the knots are marginally-resolved, non-uniform sources. The majority of sources in this zoomed-in view have colors far bluer than the typical background galaxy and are grouped in a manner to suggest that they are in fact disk objects. The physical scales of the individual knots is ~ 40 pc at the distance of NGC 3184.

To the degree the knots are resolved, our aperture corrections will underestimate the total flux. We choose the 10-pixel-diameter apertures so as to include the bulk flux from the many marginally-resolved extended sources visible in the images while not including too many neighbors (see Figure 1; false-color composite images are available from the electronic version of the paper). We set SExtractor to mask and correct neighbors that contaminate.

In our final catalog, we only include sources whose $U - V$ color error is < 0.5 mag (magnitude errors are provided by SExtractor and propagated in the standard manner). This leaves ~ 4500 sources between $1.0 - 1.5R_{25}$, the ‘outer disk region’ we examine below (the outer limit, $1.5R_{25}$, is an arbitrary choice here).

As a check of our photometry, we compare the apparent magnitudes of ten well-isolated objects across the field with those provided by SDSS-DR5, converted from u , g , and r to either V or U using the transformations of Jester et al. (2005). We find that our results are consistent with the transformed SDSS photometry to within the transformed SDSS and LBT photometric errors.

3. CLUSTER POPULATIONS SURROUNDING NGC 3184

Figure 2 shows the CMD of all detected sources between $1.0 - 1.5R_{25}$ ($R_{25} \sim 3.45$ arcmin, or ~ 11.1 kpc). Overplotted in black are Starburst99 (Leitherer et al. 1999; Vazquez & Leitherer 2005) models of fixed mass, solar metallicity star clusters covering a range in their evolutionary sequence from 1 Myr to 3 Gyr. The upper and lower tracks are of $10^4 M_{\odot}$ and $10^2 M_{\odot}$ model clusters, respectively, scaled down in mass/magnitude from a simulated $10^6 M_{\odot}$ cluster that adequately samples the Kroupa IMF. The scaled tracks are meant as

a general guide only; the stochastic sampling of the IMF at low cluster masses (Cerviño & Luridiana 2004; Fagiolini et al. 2007) is not accounted for in the following knot mass and age estimates. The uncertainties from the stochastic sampling are larger for the lower-mass and younger clusters, and a scaled-down model cluster track (from a well-sampled IMF) becomes systematically brighter and bluer than real clusters would be at a particular age (the tracks represent contributions from the highest-mass stars, which are increasingly unlikely to be found in real low-mass clusters). As a result, comparisons with the scaled model tracks can lead to underestimates of cluster masses and overestimates of their ages. Our aim here is to provide a general impression only of the cluster masses and ages consistent with the knots in our sample.

To statistically constrain the color and magnitude range of sources most likely associated with NGC 3184, we create background-subtracted Hess diagrams. A Hess diagram plots the number of sources within chosen color-magnitude bins across a CMD. The extent of the remaining signal in the background-subtracted diagrams provides an estimate of the size of the outer disk. To create these diagrams, we first produce a ‘background’ CMD from sources detected in an outer annulus between $2 - 3 R_{25}$. We also create a ‘disk+background’ CMD from the region of interest and then count the number of sources found in bins of color and magnitude (square bins of 0.2 mag were used here). We then scale the background Hess diagram to match the area on the sky represented by the disk+background Hess diagram. Finally, we subtract the scaled background Hess diagram from the disk+background Hess diagram to reveal the signal above the background.

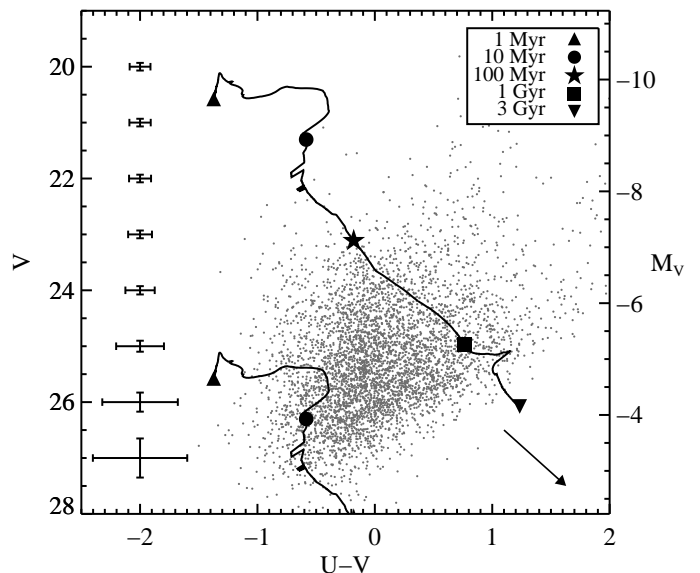


FIG. 2.— CMD of ~ 4500 sources between $1.0 - 1.5R_{25}$ from our final catalog, with median 1σ errors descending the plot at left. A reddening vector corresponding to 1 magnitude of extinction in V , calculated using results from Rieke & Lebofsky (1985), is shown at lower right. See the text for a description of the Starburst99 model tracks.

Figure 3 contains background-subtracted Hess diagrams of regions between $1.0 - 1.5 R_{25}$ and $1.3 - 1.5 R_{25}$ in the left and right panels, respectively. We use low-

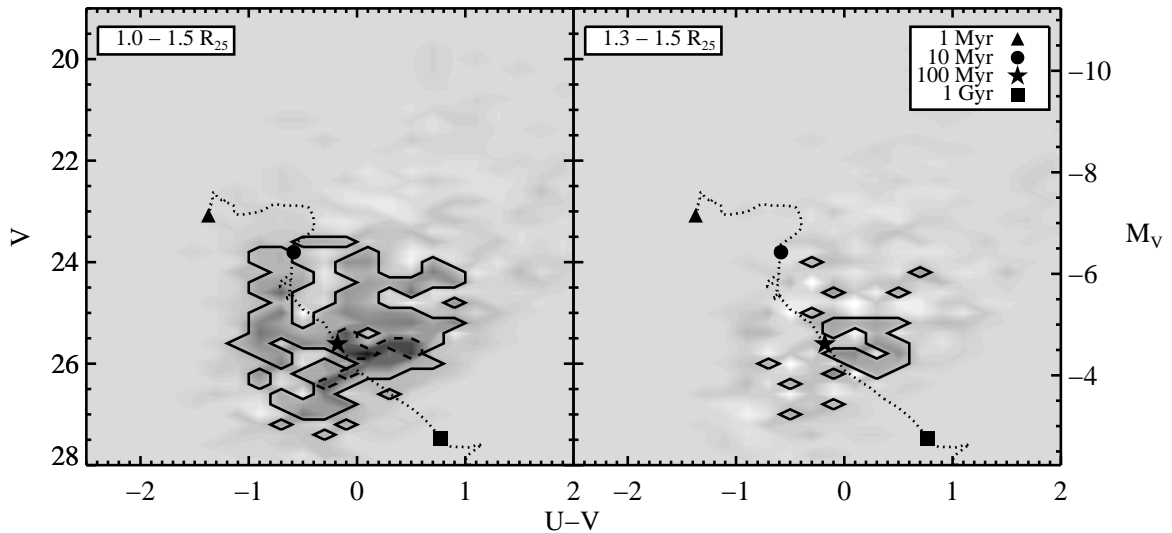


FIG. 3.— Background-subtracted Hess diagram showing the number of sources remaining between $1.0 - 1.5 R_{25}$ (left panel; dark regions are positive counts) and between $1.3 - 1.5 R_{25}$ (right panel). Solid and dashed black contours outline signal lying above the background at $> 90\%$ and $> 99.9\%$ CL, respectively. Overplotted is a $10^3 M_{\odot}$ Starburst99 model cluster, scaled down from a $10^6 M_{\odot}$ cluster as in Figure 2. *Left*: this ‘outer disk CMD’ shows a faint blue plume of sources near $U - V = -1$. The strongest signal arises from redder sources at faint levels ($V \sim 26$ mag.). From the original ~ 4500 sources in Figure 2, ~ 1100 (or $\sim 1/4$) remain after accounting for the scaled background CMD; taking the residual distribution of sources in V leads to an effective surface brightness estimate of ~ 30.3 mag arcsec $^{-2}$ for the outer disk knots. *Right*: this version only shows weak signal above 90% CL and none $> 99.9\%$ CL. In the outermost regions of the disk, it is the reddest sources that dominate by number. From the original ~ 1600 sources detected in this radial range, just ~ 200 (or $\sim 1/8$) remain; accounting for their distribution in V leads to an effective surface brightness estimate of ~ 32.1 mag arcsec $^{-2}$.

count, Poisson single-sided upper and lower limits from Gehrels (1986) to outline signal lying in excess of the background at the $> 90\%$ and $> 99.9\%$ confidence level (CL). We detect a statistically significant knot population in the outer disk of NGC 3184. The strength of the signal fades quickly with radius, and the right panel of Figure 3 suggests that $\sim 1.4 R_{25}$ is the limit of how far this method can probe the outer disk.

Although outer disk knots are typically thought of as being young because they were discovered in the UV, we find that the population of knots redward of $U - V = -0.2$ dominates that of bluer ones. The younger, blue population of knots is only detected near the optical radius with this method. However, we cannot distinguish between dust and age as the primary driver of color; we assume insignificant reddening of the majority of outer disk sources, but caution that the relative numbers of young vs. old knots is uncertain because of this issue.

In Figure 2 a $10^4 M_{\odot}$ model star cluster track for ages between 100 Myr and 1 Gyr provides an envelope for the bright end of the distribution. Above this track the number of objects falls off rapidly, implying that whatever outer disk objects are in this sample, the majority have masses $< 10^4 M_{\odot}$. Our catalog becomes incomplete for objects resembling $10^4 M_{\odot}$ clusters older than ~ 1 Gyr, and the age where this incompleteness sets in decreases quickly with decreasing cluster mass. A $100 M_{\odot}$ track suggests that at the low-mass end our final catalog is restricted to objects younger than a few tens of Myr, although this estimate is more uncertain due to the previously-discussed stochastic sampling of the IMF. Because one massive O-star forms per $200 - 300 M_{\odot}$ of stars in a cluster (Parker & Goodwin 2007, and references therein), many outer disk clusters detected here may host only a few O-stars, and many may contain none at all.

Although not well-constrained with the available optical data (i.e. V & U only), our estimated cluster mass range ($\sim 10^2 - 10^4 M_{\odot}$) matches that found in the extended disk of NGC 4625 (see Gil de Paz et al. 2005,

their Figure 4). Those authors examined GALEX FUV-selected complexes in the outer disk of NGC 4625 that also show corresponding H α emission, and found that the majority of detected knots (or clusters) lie between $10^3 - 10^4 M_{\odot}$, with the lowest-mass knots resembling $\sim 500 M_{\odot}$ clusters. A knot containing fifteen $20 M_{\odot}$ O-stars would lie just among the range of young (< 10 Myr) $\sim 10^3 M_{\odot}$ clusters (Figure 4, Gil de Paz et al. 2005), similar to what we expect to find in our images of the outer disk of NGC 3184. The distinction between our data and those from GALEX is that we have superior spatial resolution and in principle can find older clusters. The strength of the GALEX data relative to ours is that the young clusters are more prominent relative to background sources.

4. CLUSTERING OF KNOTS IN THE OUTER DISK

Another way to estimate the outer disk extent is to consider the spatial distribution of knots most likely associated with NGC 3184. Here we present correlation functions to trace the self-clustering of knots in the outer disk. To maximize whatever correlation signal exists, we must increase the contrast between the sources of interest and the background. In the FUV and NUV bands of the GALEX images, the blue star-forming knots stand out sharply against the redder background galaxies. Zaritsky & Christlein (2007) exploited this color contrast in the GALEX data and calculated the two-point correlation function of detected sources around nearby galaxies, to quantify the ubiquity of any extended disk component. Their main result was that five of the eleven galaxies studied show an excess of sources between $1.25 - 2 R_{25}$, which statistically implies that at least a quarter of such galaxies have an extended blue knot population.

We would like to use a statistical method similar to the two-point correlation analysis of Zaritsky & Christlein (2007) to measure the extent of NGC 3184’s outer disk with our LBT data. The two-point correlation approach would work well here if NGC 3184 had large numbers of

blue knots in its outer disk, because they would create the sharp color and number density contrast required to isolate them from the background. Due to the lack of blue outer disk sources, and that the dominant red sources have similar $U - V$ colors to the background objects (Figures 2 & 3), the Zaritsky & Christlein (2007) approach is not effective with our optical data. Note that a particular red color cut *can* be applied to provide enough contrast for a significant two-point correlation function to be made in the inner disk, but this correlation quickly becomes insignificant beyond R_{25} .

We must find another way to accentuate the contrast between knots and the background and thereby maximize whatever two-point correlation function signal may exist in the outer disk. As evident in Figure 1, the knots cluster about themselves. We use this self-clustering of knots as a means to provide the necessary contrast with the background; we assume that the background sources (mostly galaxies) do not cluster on scales similar to the disk objects. We then ask, ‘how far can we trace clustered knots?’

To measure the clustering of knots as a function of galactocentric distance, we calculate a ‘restricted’ three-point correlation, for which one of the 3 points is always defined to be the center of the galaxy. We begin by selecting sources by color and magnitude to have rough mass and age constraints. We then calculate the two-point knot-knot correlation at each radius. Specifically, for each knot we calculate the distance to neighboring knots (r_{out} - see Figure 4), bin the distribution of distances, and obtain an estimate of the two-point knot-knot correlation function at the galactocentric radius R of this individual knot. We repeat this process for every knot and bin in R to obtain the raw version of the restricted three-point correlation map.

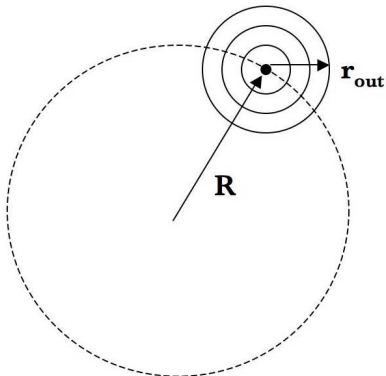


FIG. 4.— The radii defined for creating the restricted three-point correlation maps.

The raw restricted three-point correlation map must be corrected for several effects. Because we are attempting to isolate the self-clustering signal of disk-only knots as a function of radius, we must first account for contaminating correlation signal in the raw map arising from the given distribution of knots in the field at all R (both disk and background sources), as well as for contaminating signal from any spatially-correlated background galaxies. First, we normalize the two-point correlation function at each R by dividing by the number of knots at that radius, divide by the background number density of

sources calculated in an annulus at large R , and subtract 1 from the result so that the ‘unclustered’ signal is zero. Second, we correct for the underlying ‘self-correlation’ of knots across the field via Monte-Carlo simulations. Self-correlation arises because the knots are correlated with the galaxy, and so will appear correlated with each other even if the outer disk has absolutely no intrinsic clustering. To calculate and subtract this we generate 500 three-point correlation maps, similar to the original but each time randomizing the knots in angle about the galactic center. This approach preserves the source density gradient with R (which we do not wish to remove) while providing a measure of the self-correlation of a disk with no knot clustering. Subtracting the average of these 500 realizations then provides a measure of the intrinsic knot clustering. Lastly, we use the two-point correlation function at large R to subtract the underlying galaxy-galaxy correlation function (i.e. the apparent clustering of background galaxies). If there were no outer disks knots, then the correlation function along r_{out} would simply be the galaxy-galaxy correlation function and be independent of R . By subtracting the r_{out} correlation as measured at large R (beyond $2.5R_{25}$), where there presumably are no outer disk knots, we have removed the effect of contaminating galaxies. The average amplitude of the random ‘self-clustering’ correction (due to the distribution of all sources in the field) is equal to the average amplitude of the raw correlation signal at large r_{out} (> 1.5 kpc), indicating that the knots are not self-clustered on large scales. The average amplitude of the background galaxy-galaxy correction is thus also similar to the random-self-clustering-corrected signal at large r_{out} , because the signal now remaining in these regions is due only to background galaxy-galaxy clustering. At smaller r_{out} , particularly where we detect statistically-significant signal in the final map (described below), the amplitude of this galaxy-galaxy correction is negligible compared to the signal remaining from disk objects.

We use the scatter from the random realizations to set the significance level of positive excursions in the correlation map. Taking the scatter from a ‘background’ region of the random maps is insufficient, however. Due to the source distribution in the field and the different annuli area used in constructing the maps, the scatter is not uniform. From our 500 realizations we identify excursions that have only a 5% or 1% chance of occurring at that particular R, r_{out} combination. Filled contours connecting these R, r_{out} ‘pixel’ excursion values define the two-dimensional 95% and 99% significance thresholds in the map. The resulting background of noise peaks in the map (on scales of the $R - r_{out}$ binsize) can sometimes make it difficult to confidently attribute signal to actual knots clustering in the disk. In the more obscure cases, clues from the larger structure of the disk may help.

Figure 5 shows the final restricted three-point correlation signal above the 95% and 99% significance thresholds (in black and grey shading, respectively) from ‘all’ sources with $-1.7 < U - V < 0.7$ and $18 < V < 27.5$ (top panel), and from the sample split into ‘blue’ and ‘red’ on either side of $U - V = -0.2$ (middle and bottom panels, respectively). If dust significantly reddens outer disk clusters, then the strength of the correlation results presented will be underestimated for young sources and

overestimated for older sources.

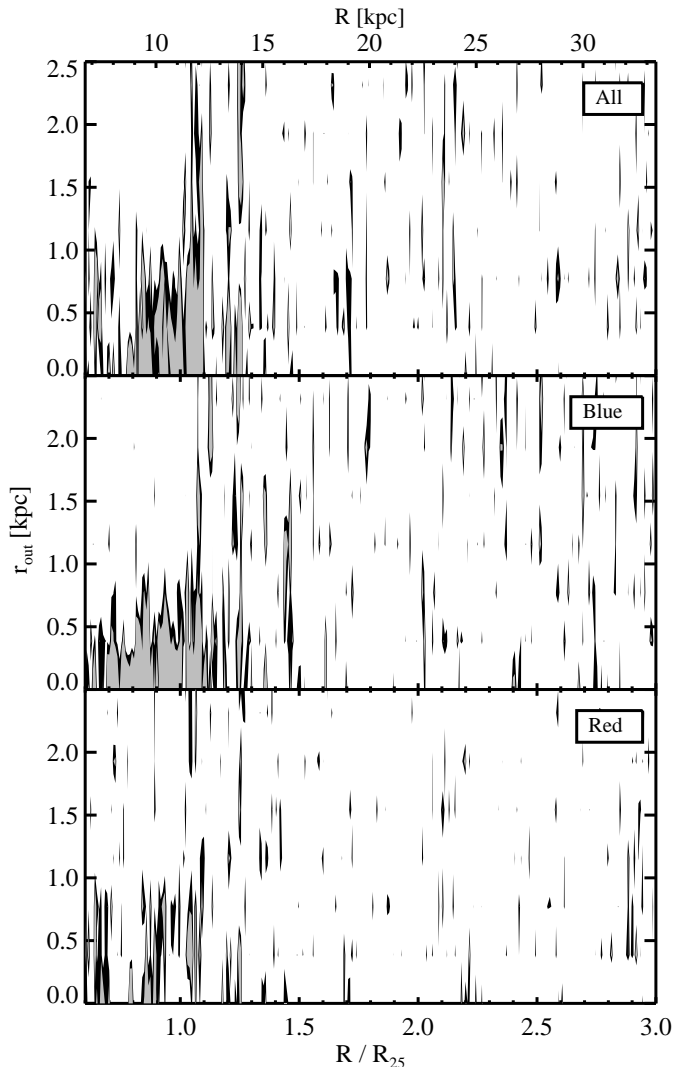


FIG. 5.— Restricted three-point correlation maps from sources in our final catalog. The top panel is from all sources with $-1.7 < U - V < 0.7$ and $18 < V < 27.5$, while the lower panels result from splitting the sample into blue and red components on either side of $U - V = -0.2$ (middle and bottom panel, respectively). Black and grey show areas where signal is detected at the $> 95\%$ and $> 99\%$ significance level, respectively, as a function of both R and r_{out} .

The choice of the red extreme in our $U - V$ color cut (0.7) was motivated by two requirements: to retain the majority of knots most likely associated with NGC 3184 while excluding the maximum number of background sources (mostly galaxies). Fukugita et al. (1995) show that the $U - V$ colors of $z = 0.2$ late-type spirals are near 0.8. Because these and earlier-type galaxies dominate the background, we chose $U - V < 0.7$ as the red extreme, with the assumption that this cut retains the majority of knots likely associated with the outer disk of NGC 3184 (Figure 2 shows that we will retain the majority of sources between $1.0 - 1.5R_{25}$). However, because galaxies become bluer in this set of filters as z increases, we expect increasing contamination from more distant galaxies. This is exacerbated by the evolution of galaxies because galaxies are typically brighter and bluer at higher redshift. Using standard Λ CDM cosmology, the

tabulated colors from Fukugita et al. (1995) and L^* from Blanton et al. (2003), we find that for $V > 23$ L^* Scd galaxies are included for $z > 0.6$. It is therefore not feasible to select a $U - V$ color cut that effectively eliminates galaxy contamination to the limits of our photometric sensitivity. Because we do not exclude all background galaxies with our color cut, we require a method to statistically distinguish knots from the background—hence the correlation map approach. It is important to note that the red cut is the only form of color contrast we use to distinguish outer disk sources from the background.

The final restricted three-point correlation maps provide another method to estimate the extent of the outer disk (the first being the background-subtracted Hess diagrams). The blue sources cluster uniformly to just beyond the optical radius, and then break into discrete aggregates that are detectable out to $\sim 1.5R_{25}$. While the red knot correlation signal is noisier, presumably due to less color distinction with the background and a less clustered distribution, there remain regions of significant clustering signal at radii comparable to those found in the blue sources. The red map is made using $\sim 1.8\times$ more sources than the blue map. Regions of increased signal along r_{out} in the blue source map (e.g. at 0.71, 0.85, 0.94, and $1.05R_{25}$) trace overdensities of knots along the spiral arms seen in the images, as do the few regions of increased signal in the red map. The regions of increased clustering signal common to both the blue and red maps near $0.9R_{25}$ and $1.05R_{25}$ can be visually attributed to large aggregates of knots seen in the images. For example, the overdensity near $1.05R_{25}$ is likely influenced by the large aggregate shown in the bottom half of Figure 1.

Due to the irregular signal in Figure 5, it is difficult to measure the radial extent of the outer disk directly from these maps. One way to better estimate the radial extent is to average the correlation signal below a chosen r_{out} and determine the R at which the average signal falls below the local averaged significance thresholds. When this is done using the fine R binning of Figure 5, a correspondingly irregular average with R is produced (not shown). Rebinning the R -annuli to be $\sim 12\times$ coarser than in Figure 5 (to ~ 1.5 kpc per bin) results in Figure 6, which presents a smoother trace of average correlation signal in R for $r_{out} \leq 0.5$ kpc. Also plotted are the corresponding average 95% and 99% significance thresholds in dotted and dashed linestyle, respectively, made from averaging similarly resampled threshold maps at regions $r_{out} \leq 0.5$ kpc to match the data map averaging. There is clustering signal in both the blue and the red knots to $\sim 1.4 - 1.5 R_{25}$. Also shown in Figure 6 are the approximate extents of the H I gas disk from two column density thresholds (see the caption and §6 for details).

Surface brightness measurements of the disk at these radii may be quite difficult. We defer a detailed surface brightness analysis of the diffuse stellar component to an upcoming paper, where we will first account for low-level scattered light in the mosaics. Here we estimate the *effective* surface brightness (eSB) of knot aggregates that can be detected in our correlation maps. We have inserted mock aggregates at different radii to determine the projected number density of knots necessary to produce a significant signal in our restricted three-point correlation maps. The mock aggregates are simply groupings of ‘detection’ locations added to the field of real knot

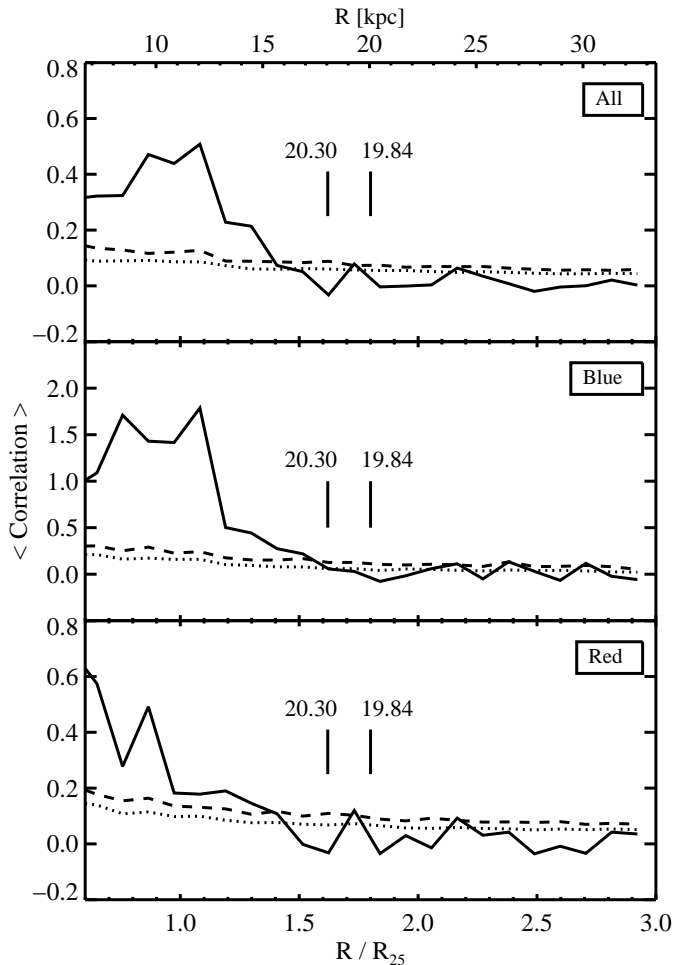


FIG. 6.— Average correlation signal from areas $r_{out} \leq 0.5$ kpc in restricted three-point correlation maps similar to those of Figure 5. The top, middle and bottom panels are from the same all, blue and red samples of Figure 5. The dotted and dashed lines mark the 95% and 99% significance thresholds, respectively. Both the blue and red sources extend globally out to $\sim 1.4\text{--}1.5R_{25}$. Also marked are the approximate radial extents of H I gas for two different boundaries, $N(\text{HI}) > 2 \times 10^{20} \text{ cm}^{-2}$ and $6.9 \times 10^{19} \text{ cm}^{-2}$, corresponding to the damped Lyman- α (DLA) system threshold and the 3σ threshold of our H I map, respectively. See §6 for more details of the H I data. The significant clustering signal from the blue knots extends nearly to the DLA system threshold.

detection locations; once a knot is counted as a detection within a particular color-magnitude cut, the shape and color of the knot are irrelevant for the construction of the correlation maps—only the locations of the detections are important. We therefore make no assumptions of the detailed shapes or colors of the fake knots, other than they satisfy the same criteria as the real knots to have made it into the final sample being considered. We find that a complex of 0.08 knots arcsec^{-2} (eight knots randomly distributed within a circular area of diameter $11''.2$) at $1.4R_{25}$ would be detected as significant signal (above the 99% significance threshold) in a map like those of Figure 5. Combining these numbers with the apparent magnitudes from our faintest detected sources (27.5 mag in V) leads us to a limiting V -band eSB of ~ 30.2 mag arcsec^{-2} for a significantly clustered aggregate at the limit of our photometric sensitivity. This eSB is similar to the outer disk eSB found from the $1\text{--}1.5R_{25}$ background-subtracted Hess diagram in Figure 3 (~ 30.3

mag arcsec^{-2}), although we caution that these estimates represent different samples of objects generated by separate methods. The eSB estimated from the outermost ~ 200 sources remaining in the $1.3\text{--}1.5R_{25}$ background-subtracted Hess diagram is ~ 32.1 mag arcsec^{-2} . For comparison (primarily to the eSBs estimated from our background-subtracted Hess diagrams), V -band outer disk eSBs estimated from star counts in M31 (Irwin et al. 2005) and NGC 300 (Bland-Hawthorn et al. 2005) are ~ 32 mag arcsec^{-2} . Low surface brightness isophote fitting is typically limited to ~ 28 mag arcsec^{-2} due to a range of technical challenges (Bland-Hawthorn et al. 2005), and so going fainter typically requires a resolved population. Our eSBs are from cluster-like knots rather than individual stars, however; NGC 3184 is too distant for detecting any but the brightest individual stars from the ground. Although we have not yet carried out a surface brightness analysis of the diffuse outer disk component of NGC 3184, we can estimate the expected surface brightness at large radii using results from the literature. Using Pompei & Natali (1997) and Godwin et al. (1977), we estimate the diffuse stellar component to be ~ 28 mag arcsec^{-2} at $1.5 R_{25}$, or $\sim 2\text{--}4$ mag brighter than the eSBs found from the knots in Figure 3.

5. A COMPARISON TO GALEX UV SOURCE EXTENT

Our three-point correlation technique can be easily applied to other datasets. Figure 7 shows the resulting correlation map when considering all GALEX UV sources near NGC 3184. The GALEX sources were collected from a search of the Multimission Archive at STScI⁷ which provides a catalog of detected sources and their associated photometry. Unfortunately the available GALEX data of this field is very limited, with only very shallow (~ 100 second) exposures from the All Sky Imaging Survey (AIS) publicly available. Figure 7 is therefore made from only the brightest knots around NGC 3184, corresponding to cluster masses of $\sim 10^4 M_{\odot}$ or larger. Because the majority of our cluster-like detections correspond to $M < 10^4 M_{\odot}$ (Figure 2), these GALEX data trace a different cluster population. We expect that the correlation map of Figure 7 would reveal structures comparable to those of Figure 5 with deeper GALEX data, although the resolution of the clustering in r_{out} would be lower due to the $\sim 6\times$ coarser spatial resolution. The correlation signal near $1.3 R_{25}$ on scales $1 < r_{out} < 2$ kpc comes from the distribution of knots just visible in the GALEX images near the outskirts of the disk, seemingly associated with extended spiral arms. The detections decline in the inner disk, presumably because it is more difficult to detect individual knots over the bright extended emission.

6. A COMPARISON TO THE UNDERLYING NEUTRAL GAS PROFILE

We now compare our estimates of the stellar/cluster disk extent to the size of the underlying gaseous disk. We begin by measuring the extent of the neutral gas disk from existing 21cm Very Large Array (VLA) imaging of NGC 3184. The beamsize of the C-configuration data is $10''$ with natural weighting (each visibility is weighted by the inverse of the noise variance, giving more weight to

⁷ MAST; <http://galex.stsci.edu/GR4>

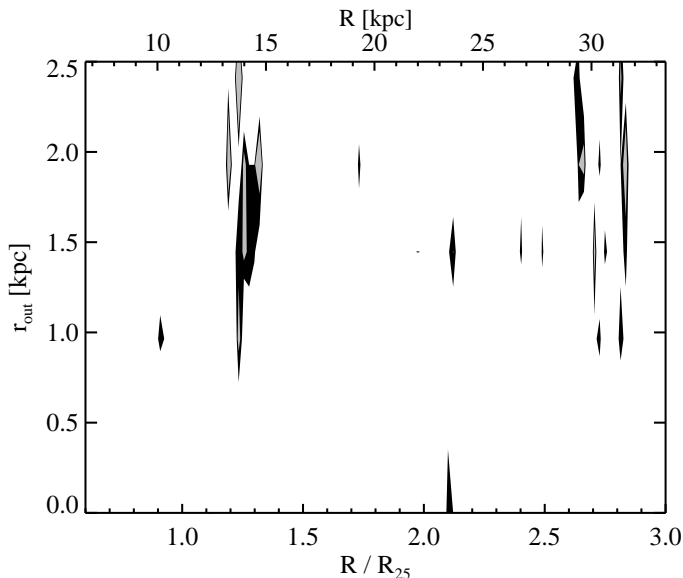


FIG. 7.— Same as Figure 5, but here using publicly-available GALEX AIS sources.

shorter baselines and larger spatial scales). The Astrophysical Image Processing System⁸ software package was used to reduce the data. Figure 8 shows the 3σ $N(\text{HI})$ extent ($N(\text{HI}) = 6.9 \times 10^{19} \text{ cm}^{-2}$) overlaid on a portion of our deep LBT V -band mosaic. To quantify the H I radial extent, Figure 9 presents histograms showing the number of H I pixels per kpc^2 above two $N(\text{HI})$ threshold values, as a function of R in $0.025R_{25}$ -wide annuli (chosen for a smooth, well-sampled trace of the decline). We use circular annuli for convenience; the inclination of NGC 3184 is 17° (Daigle et al. 2006), or nearly face-on. The top panel is of pixels with $N(\text{HI}) > 6.9 \times 10^{19} \text{ cm}^{-2}$ (the 3σ threshold and contour shown in Figure 8), and the bottom panel is of pixels with $N(\text{HI}) > 2 \times 10^{20} \text{ cm}^{-2}$. The latter value was chosen to match the damped Lyman- α (DLA) system threshold, which distinguishes between predominantly neutral and predominantly ionized gas (see Wolfe et al. 2005, and references therein). The $N(\text{HI}) = 2 \times 10^{20} \text{ cm}^{-2}$ boundary represents the edge of the dominant reservoir of neutral gas available for star formation in the disk. We estimate the gas disk extent to be $1.62R_{25}$ and $1.80R_{25}$ for the DLA and 3σ thresholds, respectively. Comparing these extents to those of the knots found using our Hess diagrams and three-point correlation maps ($\sim 1.4 - 1.5R_{25}$; Figures 3 & 6), we see that the optical disk extends at least to just below the DLA system threshold, but that the full 3σ $N(\text{HI})$ gas disk extends to larger radii.

The degree to which the extended cluster and gas disks are related can be quantified by the cross-correlation of LBT-detected knots and detected H I signal. This cross-correlation can be used as another method to trace the extent of the optical disk, in the case where the knots do not cluster about themselves but rather with the H I gas. The latter would be expected (on small r_{out} scales) if the knots formed directly from the gas in the extended disk (discussed further in §8). We construct restricted three-point cross-correlation maps in a similar manner as the knot-knot correlation maps but instead using H I

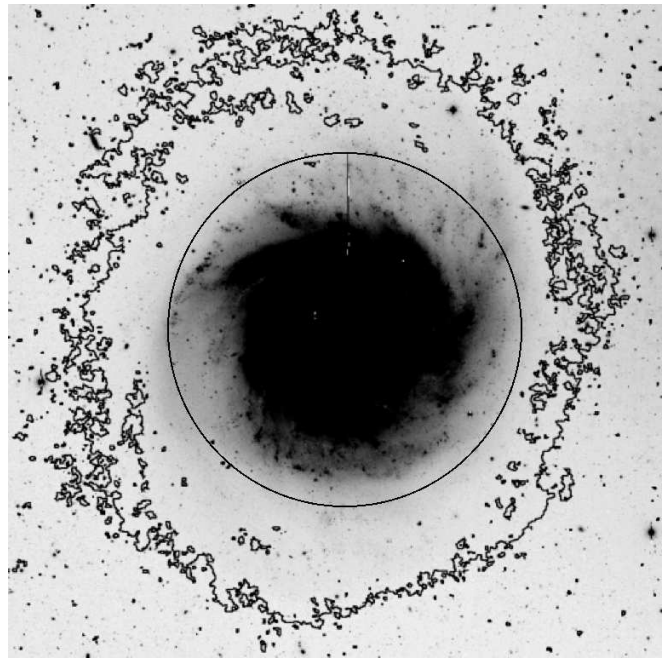


FIG. 8.— The central portion of our deep LBT/LBC V -band mosaic with the 3σ $N(\text{HI})$ threshold in black contour. This image is $\sim 3.7R_{25}$ or $\sim 12.9'$ on a side (the black circle has a radius of R_{25}). The gas disk extends beyond our detections of the outermost regions of the optical disk, as probed by our background-subtracted Hess diagrams and restricted three-point correlation maps.

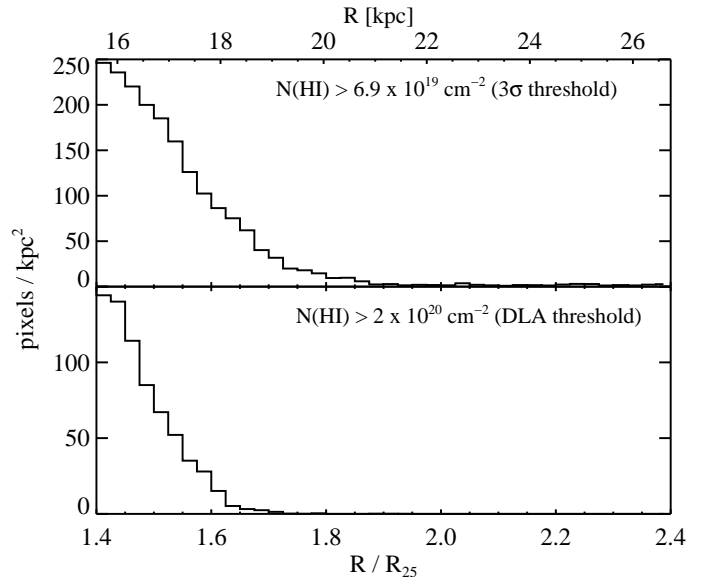


FIG. 9.— Histograms showing the number of H I pixels with $N(\text{HI}) > 6.9 \times 10^{19} \text{ cm}^{-2}$ (top) and $N(\text{HI}) > 2 \times 10^{20} \text{ cm}^{-2}$ (bottom) per kpc^2 in circular annuli of width $0.025R_{25}$. We estimate the radial extent of the H I gas above the 3σ and DLA thresholds to be $1.80R_{25}$ and $1.62R_{25}$, respectively. These extents were marked on Figure 6 to compare with the extent of clustered knots from the correlation map approach.

pixels above the 3σ $N(\text{HI})$ threshold ($6.9 \times 10^{19} \text{ cm}^{-2}$; Figure 8) as the objects surrounding a particular LBT-detected knot. We also do not subtract a background galaxy correlation signal from the maps because optical background galaxies are not correlated with the 21cm peaks in the background of the H I map. The knot-knot clustering analysis showed that the optical disk extends

⁸ AIPS; <http://www.aips.nrao.edu/>

to at least $1.4R_{25}$, so we have restricted the lower boundary of radii considered here to $1.3R_{25}$ (H I and knot data below $1.3R_{25}$ were ignored when making these maps). The upper range of the radii considered here is $2.4R_{25}$ due to the extent of available H I data. The upper, middle and lower panels of Figure 10 show the knot-H I pixel cross-correlation signal from the all, blue and red samples, respectively. We remind the reader that spurious ‘significant’ signal is to be expected across the map at the 1 – 5% level, given the large number of resolution elements in the map, and so it is sometimes difficult to know if a particular signal in a map is real. Features viewed with skepticism, especially those at large R or r_{out} , or those seen in the map of one sample (blue or red) but not in the all map, should be confirmed or refuted with further observations. Here we find strong blue knot-H I pixel clustering signal at $1.45R_{25}$ extending to $r_{out} \sim 15$ kpc, likely due to knots distributed along a tightly wound H I spiral arm seen in the H I image at $\sim 1.45R_{25}$. The red knot-H I pixel cross-correlation map shows significant extended signal near $1.73R_{25}$ between 5-10 kpc in r_{out} . This signal likely results from knots lying along another H I spiral arm near the diffuse edge of the H I pixels considered here (see Figure 8 and 9); it is however surprising that the red knots are the ones that correlate at these distances with the H I. Assuming that the cross-correlation signal at large R in the red map is real, the results of Figure 10 show that we can trace knots farther out with the knot-H I cross-correlation than with the knot-knot correlation presented in §4. While correlations with the H I on these scales are unlikely to result from in situ formation of the knots, this cross-correlation technique still provides an estimate of the radial extent of knots tracing extended spiral structure in the gas.

7. THE LOCAL ENVIRONMENT OF NGC 3184

There have been suggestions that star formation in outer disks is triggered by galactic interactions. Two of the most extended UV disks discovered by GALEX (M83 and NGC 4625, both with UV knots extending to four times their optical radii; Thilker et al. 2005; Gil de Paz et al. 2005) are both from interacting systems. Here we search the local environment of NGC 3184 for any possible perturbers.

Tully (1988) has shown that NGC 3184 belongs to a small association of galaxies consisting of three others (NGC 3104, NGC 3198 and NGC 3319). Although our optical and H I images show no obvious morphological signs of disturbance (perhaps some low-level lopsidedness in the gaseous component, see Figure 8), the H α velocity field of NGC 3184 from Daigle et al. (2006) does suggest kinematic anomalies, particularly towards the outer regions. Using the criteria of Bailin et al. (2008) to select candidate satellite galaxies most likely associated with a host, we query NED⁹ for extragalactic objects within 700 kpc of NGC 3184 (at the distance of NGC 3184, or within $\sim 215'$) and with $\Delta v < 750$ km s⁻¹ and find ten candidate satellites near NGC 3184. Seven of these ten appear to be very small and faint in SDSS-DR5 images, however, and one of the remaining three is NGC 3104, a member of the galaxy association mentioned above. Therefore, although NGC 3184 does not appear to be

⁹ <http://nedwww.ipac.caltech.edu/>

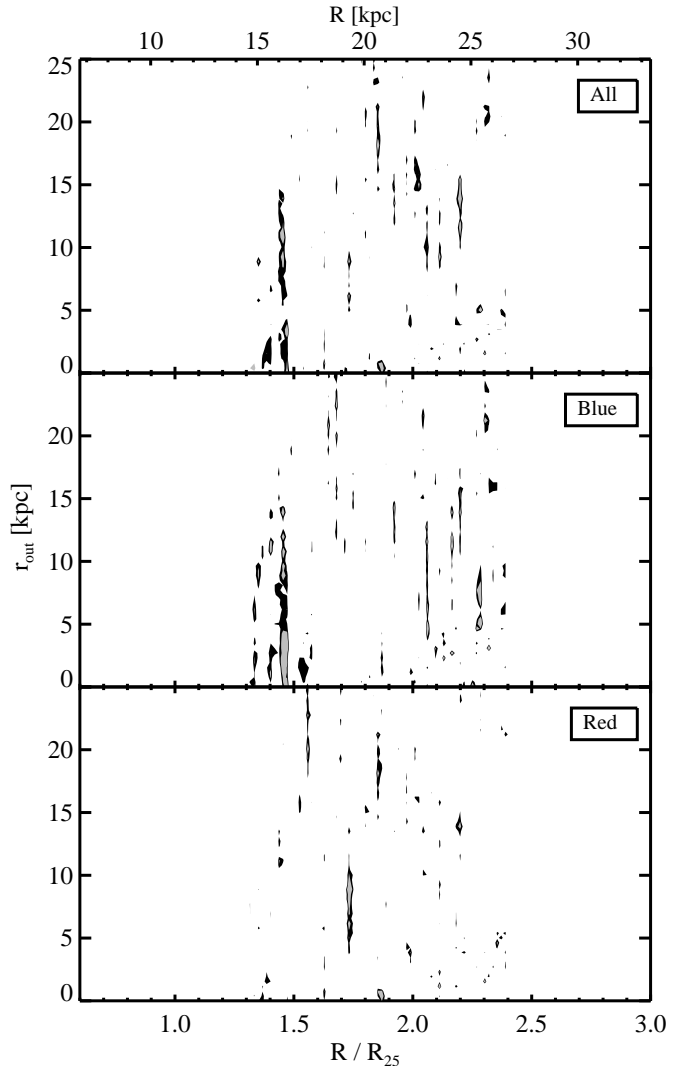


FIG. 10.— Restricted three-point cross-correlation maps of LBT-detected knots and H I pixels with $N(\text{HI}) > 6.9 \times 10^{19} \text{ cm}^{-2}$. The top panel is from all sources with $-1.7 < U - V < 0.7$ and $18 < V < 27.5$, while the lower panels result from splitting the sample into blue and red components on either side of $U - V = -0.2$ (middle and bottom panel, respectively). Only data between $1.3 - 2.4R_{25}$ were used. Black and grey show areas where signal is detected at $> 95\%$ and $> 99\%$ significance, respectively.

interacting or have had significant interactions recently (given the lack of obvious morphological disturbance), we cannot discount the possibility that previous minor perturbations have influenced the buildup of this stellar outer disk.

However, we add a final word of caution to the suggestion that interactions are required for triggering visible outer disks. Christlein & Zaritsky (2008) detect extended H α emission from a sample of nearby (edge-on) galaxies selected against nearby companions and any morphological disturbances. These results suggest that visible outer disks are a natural result of disk galaxy evolution and do not require triggering by external sources (although external disturbances may still raise the level of star formation above the nominal value).

8. SUMMARY AND DISCUSSION

We present initial results from our optical extended disk imaging study using the LBC on the LBT. We

will present a similar analysis of our full sample (nine galaxies) in a subsequent paper. Here we focus on the large, face-on galaxy NGC 3184. We find that the outer disk is populated by marginally-resolved cluster-like objects (or ‘knots’) with masses $\sim 10^2 - 10^4 M_\odot$ and ages up to ~ 1 Gyr. The cluster masses and ages are not well-constrained with the available optical data and are meant as illustrative estimates only. Background-subtracted Hess diagrams show statistically significant numbers of these cluster-like objects extending to $\sim 1.4R_{25}$, with the redder knots extending to the largest radii ($\sim 1.4 - 1.5R_{25}$). We construct restricted three-point correlation maps to measure the self-clustering of the detected knots and find significant correlation signal extending to $\sim 1.5R_{25}$. The effective surface brightness of the outer disk cluster populations we detect ranges from 30 – 32 mag arcsec $^{-2}$ in V, depending on the method and radii used for the estimate (the restricted three-point correlation map approach or background-subtracted Hess diagrams, respectively). We also present a knot-knot correlation map from GALEX-detected objects near NGC 3184 and find significant correlation near $\sim 1.2R_{25}$, although those data are currently very limited (the publically-available GALEX imaging of this field is very shallow and does not provide a large number of knots to use in the correlation analysis). We compare the 21cm H I gas disk extent to that of the knots and find that the correlated clusters extend nearly to the DLA threshold of H I gas (2×10^{20} cm $^{-2}$; $1.62R_{25}$) and are well contained within the 3σ extent of the H I gas (6.9×10^{19} cm $^{-2}$; $1.80R_{25}$). The cross-correlation between optical knots and H I pixels above the 3σ threshold suggests that the blue knots are correlated with H I spiral structure to $\sim 1.45R_{25}$, and that the red knots may be correlated with the outer fringes of the H I disk to $\sim 1.73R_{25}$. The radii at which we detect significant cross-correlation signal correspond to where we observe obvious spiral structure in the HI map, as well as a (less-obvious) enhancement of cluster aggregates tracing the spiral pattern. We therefore expect that these structures are responsible for the positive signal. Incorporating the H I data further increases our ability to detect knots associated with the disk, to the largest radii. The cluster-like objects appear to extend to the outermost reaches of the gas disk.

Assuming that knots in NGC 3184 formed in clustered aggregates of similar scales over the past few Gyr, the fact that we see continued clumpiness in the red panel of Figure 5 suggests that at least some of the original aggregates survive as a group, even after hundreds of Myr. The aggregates and knots that do dissolve, perhaps via stellar evaporation caused by encounters with neighboring clusters or giant molecular clouds (albeit on longer timescales and with lower efficiency than expected in the inner disk), may distribute many of their stars into the diffuse, low surface brightness component visible in the images (mainly as faint, extended spiral structure). This low surface brightness component is better seen in the V-band data, as expected by the numbers of red to blue clusters, the assumption that the larger ages of red sources means they have had more time to evaporate stars into a diffuse component, and simply because the

V image is deeper than the U image.

The restricted three-point correlation results illustrate how even a galaxy like NGC 3184, which appears to lack any obvious young outer disk component in both our deep exposures and the available GALEX data (albeit limited), still hosts cluster populations in its outer reaches. This suggests that the Zaritsky & Christlein (2007) and Thilker et al. (2007) estimates of the local extended UV disk fraction ($\sim 30\%$) may lie far below the local *optical* extended disk fraction.

Whether the stellar populations in the outer disk were born in situ or scattered from smaller radii is still undetermined. Roškar et al. (2008a,b) have convincingly demonstrated that stars will, over time, be scattered to larger radii and populate an outer disk of characteristics consistent with those measured from unresolved stellar populations (e.g. Pohlen et al. 2002). However, various features of our knot population suggest that these were born in situ. First, we find knot-knot clustering out to interknot separations of 1 kpc. A scattering model would presumably populate the outer disks in a much more stochastic manner. Scattering velocities would have to be coordinated to better than 10% to maintain coherence over 1 kpc while scattering objects 10 kpc from their birthsite. Second, we find correlation between the knots and the H I. The H I is clearly in a stable rotating disk and could not be scattered from smaller radii. The correlations between the two suggest a causal relationship.

A recent simulation by Bush et al. (2008) presents an in situ formation picture for the knots, showing how local overdensities of gas in an outer disk can lead to star formation closely resembling the UV knots observed by GALEX. Furthermore, Christlein & Zaritsky (2008) detect very regular outer disk rotation curves (i.e. flat, low velocity dispersion) from deep H α spectroscopy of many nearby edge-on disks, suggesting that outer disks are merely less-populated extensions of their inner counterparts (and therefore that in situ cluster formation should be expected). Given the successes of the Roškar et al. (2008a,b) studies, as well as that of Bush et al. (2008), we expect both radial migration and in situ formation to significantly influence the populations of outer disks. We encourage the modelers to identify key signatures of each mechanism that can be used to further discriminate between these possibilities. With the identification of large populations of knots, correlation statistics appears to be a promising avenue for such efforts.

We would like to thank John M. Hill and Olga Kuhn for their efforts during the LBT observations, as well as David Sand and Vincenzo Testa for helpful discussions concerning LBC data reduction and mosaicing techniques. We also thank Daniel Eisenstein for an illuminating discussion of our restricted three-point correlation map approach, and Benjamin Weiner for other helpful discussions. DZ and SHF were partially supported under NASA LTSA NNG05GE82G and NSF AST-0307482. JM acknowledges support from NASA grant 06-GALEX06-0030 and Spitzer grant G05-AR-50443.

REFERENCES

- Adelman-McCarthy, J. et al. 2007, *ApJS*, 172, 634
- Bailin, J., Power, C., Norberg, P., Zaritsky, D., Gibson, B.K. 2008, *MNRAS*, 390, 1133
- Bakos, J., Trujillo, I., Pohlen, M. 2008, *ApJL*, 683,103
- Bertin, E. 2006, in *Astronomical Data Analysis Software and Systems XV*, ASP Conf. Series 351, 112
- Bertin, E., & Arnouts, S. 1996, *A&AS*, 117, 393
- Bland-Hawthorn, J., Vlajić, M., Freeman, K.C., Draine, B.T. 2005, *ApJ*, 629, 239
- Blanton, M.R. et al. 2003, *ApJ*, 592, 819
- Bush, S.J., Cox, T.J., Hernquist, L., Thilker, D., Younger, J.D. 2008, *ApJL*, 683, 13
- Cerviño, M., & Luridiana, V. 2004, *A&A*, 413, 145
- Christlein, D., Zaritsky, D. 2008, *ApJ*, 680, 1053
- Daigle, O., Carignan, C., Amram, P., Hernandez, O., Chemin, L., Balkowski, C., Kennicutt, R. 2006, *MNRAS*, 367, 469
- Dalcanton, J.J. et al. 2008, submitted to *ApJS*
- de Jong, R.S. et al. 2007, *IAUS*, 241, 503
- de Jong, R.S. et al. 2007, *ApJL*, 667, 49
- Fagiolini, M., Raimondo, G., Degl'Innocenti, S. 2007, *A&A*, 462, 107
- Ferguson, A.M.N., Wyse, R.F.G., Gallagher, J.S., Hunter, D.A. 1998, *ApJL*, 506, 19
- Fukugita, M., Shimasaku, K., Ichikawa, T. 1995, *PASP*, 107, 945
- Gehrels, N. 1986, *ApJ*, 303,336
- Giallongo, E., et al. 2008, *A&A*, 482, 349
- Gil de Paz, A. et al. 2005, *ApJL*, 627, 29
- Gil de Paz, A. et al. 2007, *ApJS*, 173, 185
- Godwin, J.G., Bucknell, M.J., Dixon, K.L., Green, M.R., Peach, J.V., Wallis, R.E. 1977, *Obs*, 97, 238
- Gogarten, S.M. et al. 2008, arXiv0810.0266G (accepted to *ApJ*)
- Hill, J. M., Green, R. F., & Slagle, J. H. 2006, *Proc. SPIE*, 6267, 62670Y
- Irwin, M.J., Ferguson, A.M.N., Ibata, R.A., Lewis, G.F., Tanvir, N.R. 2005, *ApJL*, 628, 105
- Jester, S. et al. 2005, *AJ*, 130, 873
- Kennicutt, R.C. 1989, *ApJ*, 344, 685
- Landolt, A. U. 1992, *AJ*, 104, 340
- Leitherer, C. et al. 1999, *ApJS*, 123, 3
- Leonard, D.C. et al. 2002, *AJ*, 124, 2490
- Martin, C.L., Kennicutt, R.C., Jr. 2001, *ApJ*, 555, 301
- Martin, D.C. et al. 2005, *ApJ*, 619, 1L
- Moustakas, J. et al. 2009, in preparation
- Parker, R.J., Goodwin, S.P. 2007, *MNRAS*, 380, 1271
- Pohlen, M., Dettmar, R.-J., Lütticke, R., Aronica, G. 2002, *A&A*, 392, 807
- Pompei, E., & Natali, G. 1997, *A&AS*, 124, 129
- Ragazzoni, R. et al. 2006, *Proc. SPIE*, 6267, 626710
- Rieke, G.H., Lebofsky, M.J. 1985, *ApJ*, 288, 618
- Roškar, R., Debattista, V.P., Stinson, G.S., Quinn, T.R., Kaufmann, T., Wadsley, J. 2008, *ApJL*, 675, 65
- Roškar, R., Debattista, V.P., Quinn, T.R., Stinson, G.S., Wadsley, J. 2008, *ApJL*, 684, 79
- Thilker, D.A. et al. 2005, *ApJL*, 619, 79
- Thilker, D.A. et al. 2007, *ApJS*, 173, 538
- Tully, B. 1988, *Nearby Galaxies Catalog* (Cambridge: Cambridge University Press)
- Vazquez, G., & Leitherer, C. 2005, *ApJ*, 621, 695
- Weiner, B.J., Williams, T.B., van Gorkom, J.H., Sellwood, J.A. 2001, *ApJ*, 546, 916
- Williams, B.F. et al. 2008, arXiv:0810.2557v1 (accepted by *AJ*)
- Wolfe, A. M., Gawiser, E., Prochaska, J. X. 2005, *ARA&A*, 43, 861
- Wright, E.L. 2006, *PASP*, 118, 1711
- Zaritsky, D., & Christlein, D. 2007, *AJ*, 134, 135